



Studies on thermokinetic and reactive mechanism of graphdiyne-based NC composite via multi isoconversional methods and model reconstruction

Ningning Zhao · Ergang Yao · Haixia Ma · Jianyou Zeng · Zhong Yu · Ting An · Fengqi Zhao · Xiaojiao Yu

Received: 15 September 2021 / Accepted: 29 March 2022 / Published online: 22 April 2022
© The Author(s), under exclusive licence to Springer Nature B.V. 2022

Abstract In this work, graphdiyne (GDY) is used for the first time as the catalyst for the pyrolysis process of nitrocellulose (NC). By DSC and TG-IR-MS results, the compatibility and the possible catalytic mechanism of GDY on NC are investigated. The kinetic triplet parameters of the GDY/NC complexes were determined based on the isoconversional analysis (using the KAS, FWO, and Friedman methods), whereas the experimental reaction model of the GDY/NC pyrolysis was optimized and re-established by introducing a newly modified function with result of $f(\alpha) = 9.138\alpha^{0.838}(1-\alpha)^{2.343}$. Compared with pristine NC, the GDY/NC complexes exhibit a lower peak temperature, an increased heat release, and a lower energy barrier, owing to the good catalytic characteristics of GDY. This was also demonstrated via the

TG-IR-MS measurements, which revealed how GDY accelerates the rupture of the $-O-NO_2$ bond and the secondary self-catalytic reaction.

Keywords GDY/NC · Catalytic activity · Kinetic triplet · Model reconstruction · TG-IR-MS

Introduction

Lightweight carbon materials possess superior optical properties, thermal stability, radiation resistance, catalytic ability, electrical insulation, conductivity, surface activity. These beneficial characteristics are the motivation for the wide application of lightweight carbon materials to the fields of hydrogen storage (Samantaray et al. 2020; Shi et al. 2020a), electronic devices (Ashery et al. 2020; Zhang et al. 2017a) (including new electron probes, supercapacitors (Wong et al. 2020; Zhou et al. 2020; Hao et al. 2021), field-emission electron guns, and electrode materials (Liu et al. 2021a; Ma et al. 2021, 2020)), life sciences, biomedicine (Ahlawat et al. 2020), astrophysics, water splitting (Koo et al. 2018), etc. In civil and military fields, they can be used as thermal igniters (Kim et al. 2017), photocatalyst or adsorbents for special pollutants (Yi et al. 2018), military protective clothing, electromagnetic absorption materials (Chen et al. 2018, 2019a), catalytic materials (Wang et al. 2012a), energetic components (van der Heijden et al. 2003), etc. Traditional sp^2 hybrid carbon materials such as

Supplementary Information The online version contains supplementary material available at <https://doi.org/10.1007/s10570-022-04569-8>.

N. Zhao (✉) · Z. Yu · X. Yu
School of Science, Xi'an University of Technology,
Xi'an 710054, Shaanxi, China
e-mail: zhaonn@xaut.edu.cn

E. Yao · T. An · F. Zhao
Science and Technology on Combustion and Explosion
Laboratory, Xi'an Modern Chemistry Research Institute,
Xi'an 710065, Shaanxi, China

H. Ma · J. Zeng
School of Chemical Engineering, Northwest University,
Xi'an 710069, Shaanxi, China

carbon nanotubes, fullerenes, graphene and its derivatives, are able to modify the heat release of energetic materials (Zhao et al. 2016a; Xu et al. 2017a; Yuan et al. 2014; Chen et al. 2016; Zu et al. 2016; Zhang et al. 2014). Due to the unique structure and excellent properties of carbon materials, the development of their fundamental research and application technology is highly valued by governments, academia, and industry all over the world. Furthermore, new types of carbon allotropes are constantly emerging, which is attracting considerable attention.

Graphdiyne (GDY), a new two-dimensional all-carbon nanostructured material, possesses high π -conjugation system of sp/sp^2 hybrid carbon atoms, a tunable bandgap, distinct nanotopological pores, and numerous active sites (Xue et al. 2016), which could result in an excellent catalytic activity (Sun et al. 2021; Song et al. 2020), a remarkable electrical conductivity (He et al. 2017), a high chemical stability, an effective mass transport, and good mechanical properties. Since its first synthesis in 2010 (Li et al. 2010), GDY has attracted increasing attention in numerous fields, such as water splitting (Liu et al. 2021b; Lv et al. 2020; Shi et al. 2020b), energy conversion and storage (Gao et al. 2020a; Lin et al. 2020), catalysts (Yin et al. 2020; Wang et al. 2020), gas generation (Liu et al. 2020), gas separation (Mahdizadeh and Goharshadi 2020), and sensors (Cui et al. 2020). However, to the best of our knowledge, no studies have been conducted on the use of GDY-based catalysts in the field of the cellulose-derived energetic polymers.

Investigations on cellulose-derived energetic polymers, such as nitrocellulose (NC), provide an important basis for the development of next-generation energetic formulations, such as propellants and explosives (Tarchoun et al. 2020a, 2020b, 2020c, 2021a, 2021b, 2022). Being a main energetic ingredient of NC-based energetic materials, NC is widely employed in conjunction with fuels, adhesives, modifiers or catalysts, plasticizers, curing agents, stabilizers, and other additives in both civilian and military fields. It has been widely studied to improve the energetic features of NC-based energetic materials and apply catalytic activity to thermal degradation by using catalysts in the recent years. In an effort to understand of the thermal behavior, reaction kinetics, and thermocatalytic decomposition, various analytical techniques such as differential scanning

calorimetry (DSC) technique or thermogravimetric analysis (TGA), as well as thermogravimetry (TG) coupled with either infrared spectroscopy (TG-IR) or mass spectroscopy (TG-MS) (Benhammada and Trache 2020) have been employed.

Herein, GDY was used for the first time as the catalyst to improve the thermolysis process of NC and investigate its catalytic mechanisms. The thermal behavior and thermokinetic of the GDY/NC complexes were evaluated based on the DSC data, where the kinetic triplets were determined through the KAS, FWO, and Friedman isoconversional analysis methods, whereas the reaction model was optimized and reconstructed using a modified theoretical function. Finally, the TG-IR-MS simultaneous technique was used to detect the produced gases or fragments and deduce the possible catalytic mechanism of GDY. The insights thus gained can be instructive for the development of novel extremely reliable and highly active GDY-based catalysts for use in the field of energetic materials.

Experimental materials and methods

Preparation of the GDY/NC mixture

GDY was prepared according to the reference (Li et al. 2010). GDY/NC complexes composed of GDY (as the catalyst) and NC (12.6 N%) with a mass ratio of 1:19 were obtained through a 20-min grinding treatment at ambient temperature. GDY/NC (1/1 w.%) mixtures with a 1:1 (w/w) ratio were prepared for compatibility investigations, respectively according to the NATO Standardization Agreement STANAG 4147 (Chelouche et al. 2019a, 2019b) and the evaluated standards reported in references (Beach and Canfield 1971; Yan et al. 2008).

Characterization

Scanning electron microscopy (SEM, Zeiss SIGMA), transmission electron microscopy (TEM, FEI Tecnai G2 F20), energy dispersive X-ray spectroscopy (EDS, INCAIE350), X-ray diffraction (XRD, D/MAX-3C), X-ray photoelectric spectroscopy (XPS, Thermo Scientific K-Alpha) and Raman spectroscopy (Renishaw in Via Reflex) were used to study the morphology, microstructure and composition of GDY. The

compatibility and thermal behavior were evaluated via DSC (Q2000 TA) from ambient temperature to 300 °C at the heating rates of 2.0 and 10.0 K·min⁻¹ in flowing nitrogen (50 mL·min⁻¹). Furthermore, the kinetic triplet parameters, including the activation energy (E_α), pre-exponential factor (A), and reaction model ($f(\alpha)$), were mathematically modeled based on the DSC data at six different heating rates. The gases produced from the whole thermolysis processes of the as-prepared materials were detected by TG (Mettler Toledo TGA/DSC 3+(HT)), Fourier-transform IR spectroscopy, and quadrupole mass spectrometry (QMS 403 C Aëolos) (i. e., the TG-IR-MS technique) in purified argon at a heating rate of 10.0 K·min⁻¹.

Isoconversional methods

The Kinetics Committee of the International Confederation for Thermal Analysis and Calorimetry (ICTAC) (Vyazovkin et al. 2011; Vyazovkin 2018) recommends the use of the isoconversional kinetic analysis for obtaining reliable kinetic parameters without assuming any reaction model. The KAS (Kissinger 1957; Akahira and Sunose 1971), FWO (Flynn and Wall 1966; Ozawa 1965), and Friedman (Sánchez-Jiménez et al. 2013; Xu et al. 2017b; Friedman 1964) isoconversional methods, which are described by Eqs. (1)–(3) respectively, were employed to estimate the kinetic triplets of NC and the GDY/NC complexes.

$$\ln \frac{\beta_i}{T_{\alpha,i}^2} = \ln \left(\frac{AR}{E_\alpha G(\alpha)} \right) - \frac{E_\alpha}{RT_{\alpha,i}} \quad (1)$$

$$\ln \beta_i = \ln \left(\frac{AE_\alpha}{RG(\alpha)} \right) - 5.3305 - 1.052 \left(\frac{E_\alpha}{RT_{\alpha,i}} \right) \quad (2)$$

$$\ln \left[\beta_i \left(\frac{d\alpha}{dT} \right)_{\alpha,i} \right] = \ln [Af(\alpha)] - \frac{E_\alpha}{RT_{\alpha,i}} \quad (3)$$

In these equations, the subscript i is i th heating rate, $T_{\alpha,i}$ is the temperature at which the extent of conversion α is reached under the i th temperature program, $G(\alpha)$ is the integral form of the reaction model (Cai et al. 2018), and $f(\alpha)$ represents the reaction rate dependence on conversion rate (α). The $f(\alpha)$ kinetic functions listed in Table S1 in the Supplementary Material are associated with different physical models

that describe the kinetic mechanisms of solid-state processes (Sánchez-Jiménez et al. 2010a).

Results and discussion

Structural analysis

The microstructure and composition of the GDY films were characterized by SEM, TEM, EDS, XRD, XPS and Raman spectroscopy. The SEM image presented in Fig. 1a shows that the as-prepared GDY films display multilayer structures with curly edges and a rough surface. Figure 1b displays that the GDY film is not a single-layer structure but rather a multilayer film. The HRTEM image of the GDY film is illustrated in Fig. 1c. It can be inferred that the layer-to-layer distance was 0.365 nm. The HRTEM image (Fig. 1c), selected area electron diffraction (SAED, Fig. 1d) and XRD pattern (Fig. 1f) reveal that the GDY film has an amorphous structure. The two sharp peaks in the EDS pattern in Fig. 1e demonstrate that the GDY film was mainly composed of carbon and oxygen elements. The O element originates from the air adsorbed on the GDY film. Figure 1g presents that the GDY film is mainly composed of C, O, and N elements. The presence of oxygen and nitrogen elements might result from the absorption of air or the presence of inevitable defects. The high-resolution C 1s XPS spectrum of GDY displayed in Fig. 1h can be deconvoluted into four subpeaks with binding energies of 284.5, 285.3, 286.9 and 288.5 eV, which are attributed to C–C (sp²), C–C (sp), C–O, and C=O (Chen et al. 2019b), respectively. The area ratio of the sp-hybridized carbon to the sp²-hybridized carbon is approximately 2.0 (Wang et al. 2012b), which reveals that the benzene rings in the GDY structures could be connected to each other via conjugated diyne linkers. In the typical Raman spectrum of GDY (Fig. S1), the characteristic peaks at 1356.6 and 1587.8 cm⁻¹ are assigned to the D and G bands, respectively, whereas the weak peaks at 1937.8 and 2185.8 cm⁻¹ are the vibrations of the acetylenic (–C≡C–) and diyne (–C≡C–C≡C–) linkage, respectively (Zuo et al. 2017).

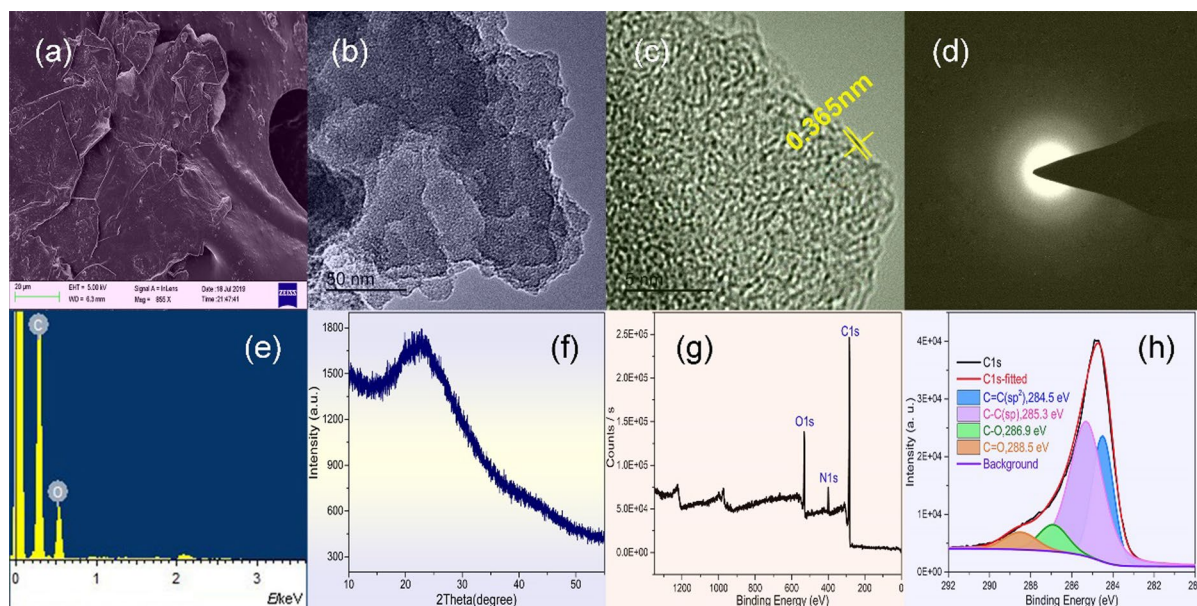


Fig. 1 **a** SEM micrograph, **b** low-magnification TEM image, **c** HRTEM image, **d** SAED pattern, **e** EDS pattern, **f** XRD pattern, **g** XPS spectrum (survey) and **h** XPS C 1s spectrum of GDY

Compatibility and thermal behavior

The DSC thermal analysis method is widely used to assess the compatibility between the explosive and various contacted ingredients due to its attractive features, such as less sample usage, low cost, and operation convenience. The peak temperature values of the pyrolysis processes of pure NC and GDY/NC (1/1 w.%) mixtures were measured at the heating rates of 2.0 and 10.0 K·min⁻¹ respectively, and the results were presented in Table S2. According to the STANAG 4147 criteria (Li et al. 2016), the exothermic decomposition temperature of GDY/NC (1/1 w.%) is 466.3 K, which is 1.2 K lower than that of pure NC. Therefore, GDY/NC (1/1 w.%) can be considered compatible because the maximum exothermic peak temperature difference between NC and GDY/NC (1/1 w.%) is less than 4 K. Another evaluated standard of compatibility for explosive and contacted materials is performed at DSC heating rate $\beta = 10.0$ K·min⁻¹ (Beach and Canfield 1971; Yan et al. 2008). According to this criterion, the GDY/NC mixture can also be regarded as compatible and safe for use in the explosive design, because the value of ΔT_p is lower than 2 K (shown in Table S2).

Typical DSC curves in Fig. 2 show that the thermal decompositions of the analyzed samples possess only one exothermic peak. The exothermic peak belonging to the pyrolysis phenomenon of NC-based composites was widely reported. Yet the values of the decomposition temperatures exhibited some variations (shown in Table S3) for NC-based composites because of

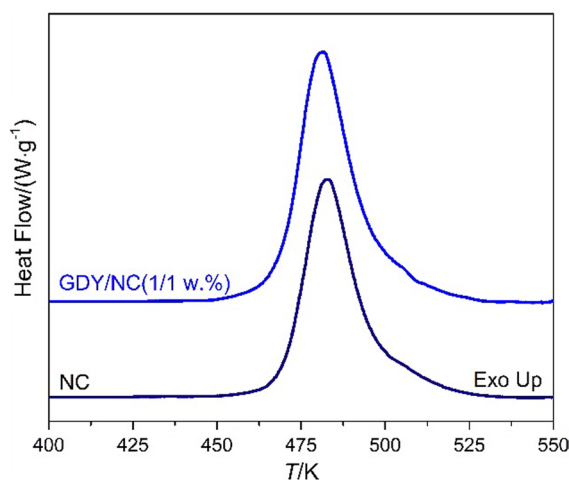


Fig. 2 DSC curves of the GDY/NC (1/1 w.%) mixtures and NC obtained at a heating rate of 10.0 K·min⁻¹

the differences in the composition of samples, the nitrogen content of NC, the additives, the analytical technique, and the measurement uncertainty. Thermal properties, including the peak temperature and the heat release, were assessed by using the repeated DSC measurements in order to make the results (shown in Table S4) more accurate and credible. The GDY/NC (1/1 w.%) mixtures exhibit a 1.1 K-lower peak temperature than pure NC; yet, the heat release is increased by $460.6 \text{ J}\cdot\text{g}^{-1}$ (24.3%), which indicates that the GDY films can be used as catalyst and have an impact on the pyrolysis behavior of NC.

Kinetic analysis and model reconstruction

The kinetic triplets (E_α , A , and $f(\alpha)$) of the GDY/NC complexes and NC are obtained based on the DSC data at six different heating rates (namely 5.0, 10.0, 15.0, 20.0, 25.0, and 30.0 $\text{K}\cdot\text{min}^{-1}$). Figure 3 shows that the different heating rates have a pronounced influence on the thermolysis process of NC; indeed, it can be observed that the temperatures shifted toward higher values upon increasing the heating rate (Tarchoun et al. 2019; Chai et al. 2019).

Kinetic isoconversional methods are reliable approaches, which are recommended by the ICTAC Kinetics Committee. FWO, KAS, and Friedman equations are employed to obtain the activation energy. The results of the simultaneous analysis carried out

using the FWO, KAS, and Friedman equations for the experimental data are shown in Fig. 3, and the obtaining curves are shown in Fig. 4. It can be seen that the straight lines are approximately parallel; in particular, the trend of the FWO isoconversional curve is overall consistent with that of the KAS curve. The Friedman isoconversional curve displays slightly different trend due to the approximations (Xu et al. 2017b) adopted in the algorithms. Therefore, the E_α values calculated using the Friedman method are slightly higher than those calculated using the FWO and KAS methods, as can be seen in Fig. 5.

The E_α values as a function of α could be estimated from the slopes (k) of the KAS, FWO, and Friedman curves. Figure 5 shows the obtained E_α values and confidence intervals (errors bars) as well as their variation with α . Figure 5a presents the variation of E_α for GDY/NC at each conversion rate α (from 0.025 to 0.975) calculated using the FWO, KAS, and Friedman isoconversional methods. The E_α values increase with increasing α from 148.6 ± 17.1 to $212.5 \pm 29.6 \text{ kJ}\cdot\text{mol}^{-1}$ and from 148.6 ± 18.0 to $215.0 \pm 31.2 \text{ kJ}\cdot\text{mol}^{-1}$ for the FWO and KAS methods, respectively. The E_α values of GDY/NC obtained using the Friedman method are relatively low due to the autocatalytic characteristics of NC and the catalytic properties of GDY at the beginning of the reaction within the α range of 0–0.025. The thermal decomposition starts slowly at the beginning, and

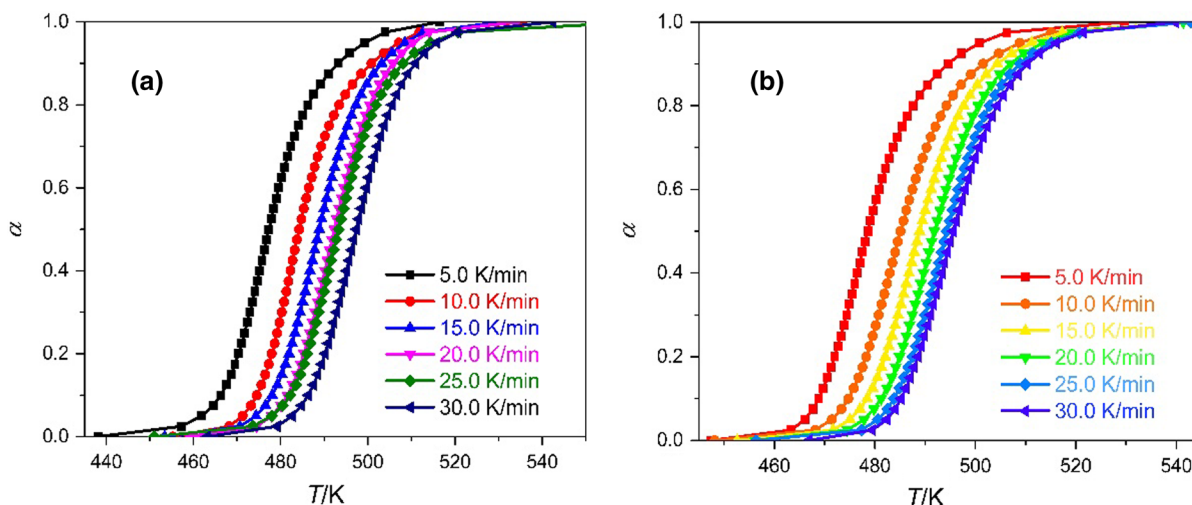


Fig. 3 Experimental curves obtained for the thermal decomposition of GDY/NC (a) and NC (b) in N_2 atmosphere with the linear heating rate of 5.0, 10.0, 15.0, 20.0, 25.0 and 30.0 $\text{K}\cdot\text{min}^{-1}$

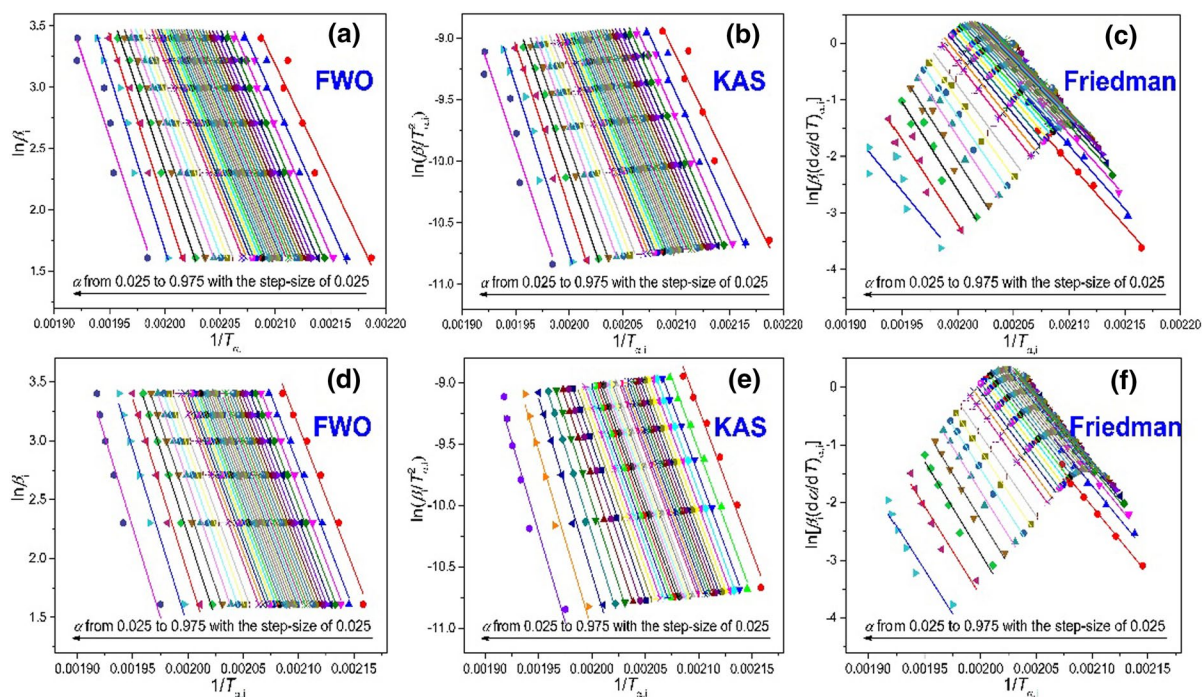


Fig. 4 Global kinetic plots of GDY/NC (a–c) and NC (d–f) based on FWO, KAS and Friedman methods

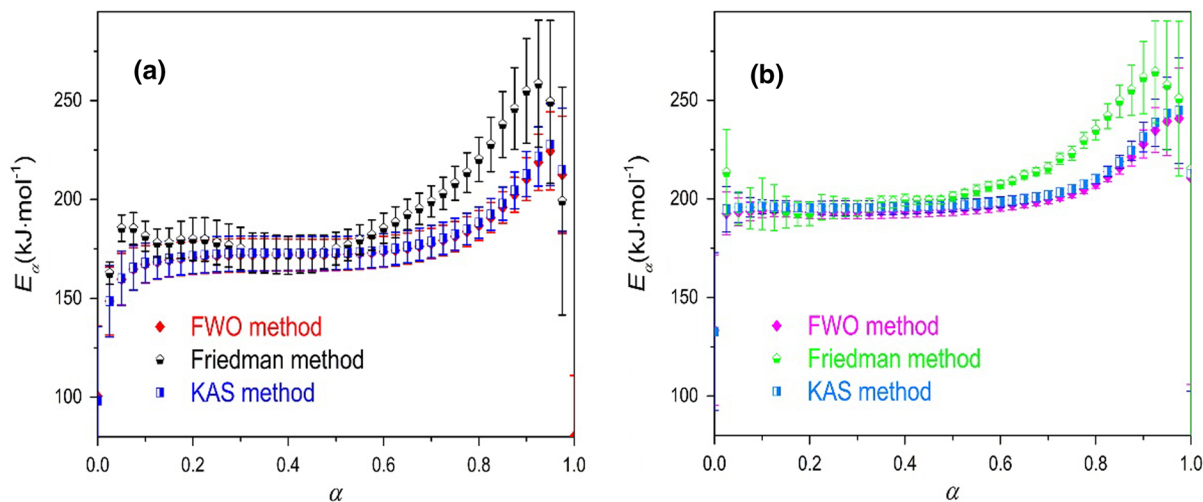


Fig. 5 Activation energy (E_α) and the associated error evolution with respect to the conversion rate (α) obtained by the three employed isoconversional methods for GDY/NC (a) and NC (b)

the reaction rate increases rapidly with the accumulation of the catalytic products. The E_α values obtained using the Friedman method decrease (with fluctuations) with increasing α in the α range of

0.05–0.4, reaching the lowest value at $\alpha=0.4$, and then increasing slightly (with fluctuations). The E_α values are high at the beginning of the pyrolysis process of GDY/NC, which is attributing to the

–O–NO₂ bonds cleavage in NC and the formation of NO₂. For $\alpha > 0.05$, E_α decreases from 185.4 ± 6.7 to 171.8 ± 9.7 kJ·mol⁻¹ until $\alpha \approx 0.4$ is reached; this decrease is possibly caused by the catalysis effect of GDY. Moreover, as the temperature increases, the production of gas products and small molecular fragments will affect the thermal decomposition of GDY/NC, resulting in an increase in the activation energy. For $\alpha = 0.05$ – 0.925 , all the values of the linear correlation coefficient (R^2) exceed 0.92, revealing that the obtained activation energies are quite accurate. However, a significant deviation presents at α values over 0.925, which is accompanied by large standard errors and a weak linear dependence. These variations can be explained in terms of several complex steps, including the pyrolysis of the residues and the effect of the escaped gaseous products.

The average values of the Arrhenius parameters alongside their standard deviations obtained by the three isoconversional equations are provided in Table 1. Compared with the E_α values calculated using the FWO, KAS, and Friedman isoconversional approaches for NC, the E_α values of GDY/NC decreased by 28.1, 28.8, and 25.8 kJ·mol⁻¹, respectively, indicating that GDY/NC has a lower thermal stability than pure NC. This finding shows that the GDY specificity is different from that of other lightweight carbon materials, such as carbon nanotube (Smeu et al. 2011) and graphene oxide (Zhang et al. 2013); this results in improved thermal decomposition pathways and regulates the energy release from energetic materials. The development of efficient and new additives (e.g., nanometal oxides, nanothermites, nanocomposites, and eutectics) for improving the degradation of NC-based energetic materials has received significant attention. Table S3 summarizes the kinetic parameters for the pyrolysis of NC and NC-based composites reported in recent works. Trache et al. reported CuO (Benhammad and Trache

2022) and Fe₂O₃ with various grain sizes (Benhammad et al. 2020) and found that Fe₂O₃-CMS composites (Trache et al. 2016) have a significant influence on the thermal decomposition of NC. In Particular, the E_α value of Fe₂O₃-CMS-NC decreased by 12.9 kJ·mol⁻¹, indicating the good catalytic activity of the Fe₂O₃-CMS particles on the decomposition behavior of NC. In other studies, CuO (Zhao et al. 2021), Fe₂O₃ (Zhao et al. 2016b), Cr₂O₃ (Guo et al. 2019), Al/CuO (Yao et al. 2020), Al/Fe₂O₃ (Zhang et al. 2017b), ZIF-8 and CuO/ZIF-8 (Zhao et al. 2022) were found to accelerate the pyrolysis process of NC by reducing the energy barrier. Actually, the differences in the obtained E_α values for pure NC and the NC-based composites are due to the different experimental conditions, the catalysts used, the analytical techniques, and the kinetic modeling approaches. According to the STANAG 4147 criteria, the activation energies of mixtures (explosive + additive) prepared in a ratio of 1:1 (w/w) should be calculated from the peak temperatures and heating rates by the Kissinger method. Calculated values are listed in Table S4, for the GDY/NC (1/1 wt.%) system, a small shift (1.5%) in activation energy to a little lower value compared to that found for pure NC indicating a compatibility between GDY and NC.

The different kinetic models presented in Table S1 do not always accurately describe the thermal decomposition in solid materials with or without porous structures (Gao et al. 2020b). Figure 6 shows a comparison of the normalized function curves of the theoretical kinetic models and experimental master curves for NC with and without GDY. It can be seen that the experimental master curves obtained at the six different heating rates are slightly similar to the theoretical curves corresponding to the random scission (L2) model (Sánchez-Jiménez et al. 2011) for $\alpha < 0.5$ and the three-dimensional diffusion (D3) model for $\alpha > 0.5$. The L2 model is typically used to describe

Table 1 Kinetic parameters for GDY/NC complexes and NC pyrolysis

Samples	Methods	E_α /(kJ·mol ⁻¹)	lg(A/s ⁻¹)	$f(\alpha)$
GDY/NC	FWO	173.3 ± 8.6	19.5 ± 0.9	9.138α ^{0.838} (1-α) ^{2.343}
	KAS	175.0 ± 8.8	18.6 ± 0.9	
	Friedman	186.3 ± 9.5	20.6 ± 1.7	
NC	FWO	201.4 ± 4.6	21.2 ± 1.8	8.792α ^{0.762} (1-α) ^{2.359}
	KAS	203.8 ± 4.8	21.1 ± 1.8	
	Friedman	212.1 ± 6.6	22.5 ± 1.5	

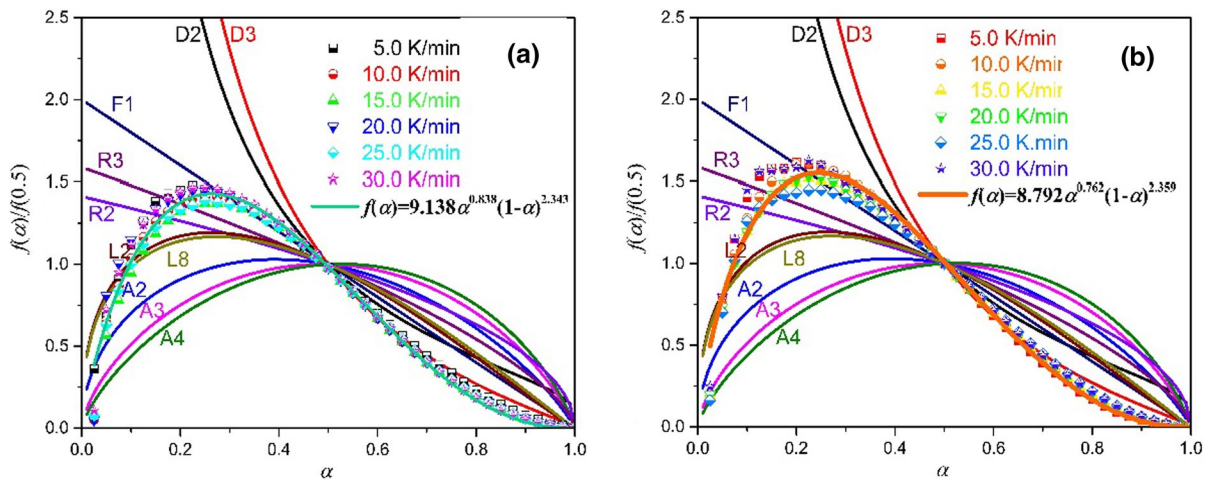


Fig. 6 Comparison between normalized curves of obtained kinetic models for GDY/NC (a) and NC (b) and theoretical master curves constructed from the ideal kinetic models in Table S1

the polymer degradation reactions (Sánchez-Jiménez et al. 2010b). However, it should be pointed out that the pyrolysis processes of the real GDY/NC and NC systems deviate from such an ideal theoretical model, which is established by imposing restrictions on the homogeneity and geometry of the material as well as the force driving the reaction. The D3 model is based on the assumption of spherical solid particles (Kha-wam and Flanagan 2006), which is not completely adequate for NC or NC-based composites. Therefore, even L2 and D3 models that provide the best fit are not entirely compatible with the experimental master curves. This conclusion can also be inferred by investigating the kinetic compensation effect (KCE), which describes the linear relation between E_α and the pre-exponential factor. Figures 7a and b present a comparison of the kinetic compensation lines for the thermal decomposition processes of GDY/NC and NC. However, this linear correlation is not ideal; in particular, the R^2 value of the fitting curve for NC is only 0.89973. The KCE results, which are shown in Fig. 7, also demonstrate that the selected L2 and D3 models are not fully adequate to describe the pyrolysis reactions of GDY/NC and NC.

In order to understand the mechanisms underpinning the effect of GDY on the NC thermolysis, the physical models of GDY/NC are evaluated. When reconstructing the reaction model to obtain a good fit with the experimental data, the modified Šesták–Berggren empirical equation described in

Eq. (4) was employed based on the combined kinetic analysis method.

$$f(\alpha) = c\alpha^m(1 - \alpha)^n \quad (4)$$

By adjusting the parameters c , m and n and the possible deviations from the ideal conditions, Eq. (4) was found to be able to fit the common physical models (Ma et al. 2019). The results in Fig. 7 suggest that the experimental curves and the modified theoretical master curves are matching well with three constants c , m , and n to achieve the kinetic reaction models finally. The kinetic models of GDY/NC and NC can be described by quantitative equations (Table 1) as shown in Fig. 6. It can be found that the modified theoretical models are in highly accordance with the corresponding experimental data, as also demonstrated by Figs. 7c and d. As Figs. 7c and d show, the slopes and intercepts of the two straight lines are different, indicating that GDY has a catalytic influence on the pyrolysis of NC. Based on the model reconstruction, the thermolysis processes of GDY/NC and NC are predominantly controlled by the modified n -order kinetic models.

TG-IR-MS analysis

The whole thermal decomposition process and gaseous products were investigated using the TG-IR-MS technique. From the TG/DTG curves in Fig. 8a,

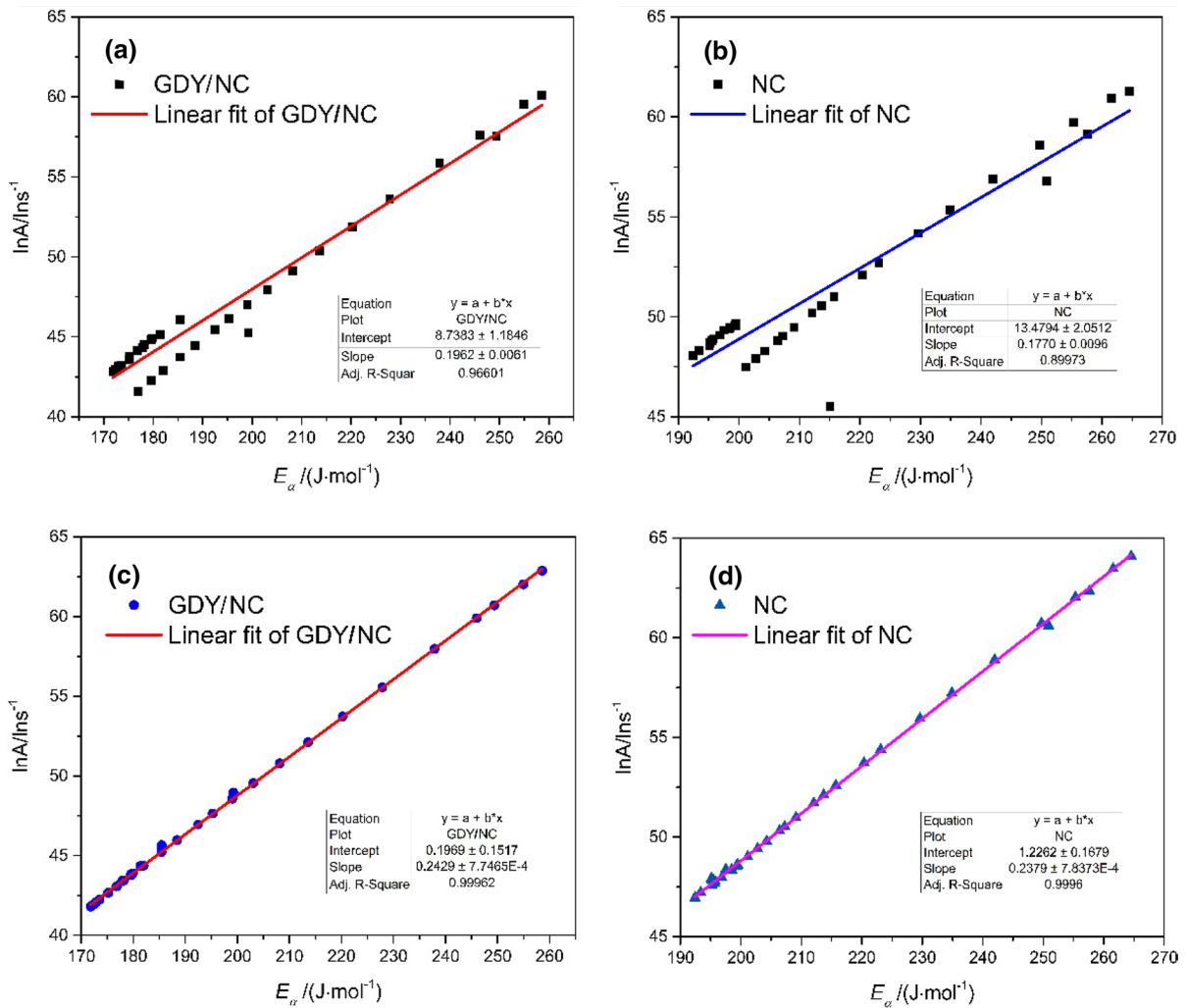


Fig. 7 Kinetic compensation effect for pyrolysis of GDY/NC and NC calculated by isoconversional method (a,b) and the combined kinetic analysis method (c,d) within conversion range from 0.025 to 0.975

it can be observed that the GDY/NC complex exhibits only one thermogravimetric stage, which takes place in the temperature range of 449.8–520.4 K, with a maximum degradation rate at 477.8 K and a weight loss of 75.6 wt%. For GDY/NC, it is a mixture of 5.0 wt% GDY and 95.0 wt% NC. Additionally, the total mass loss of pure GDY is only around 1.2% at 477.8 K (Zeng et al. 2021). This indicates that the total weightlessness quantity of GDY/NC can be mainly attributed to the thermal decomposition of NC. By comparing the results shown in Fig. 8 with those reported in our previous work on NC thermal degradation (Zhao et al. 2016c), it can be found that the temperatures corresponding to

the initial decomposition (T_i), extrapolated onset of degradation (T_o), maximum degradation rate (T_p), extrapolated end of degradation (T_e), and end of the reaction (T_f) for the GDY/NC composites are shifted toward lower values, indicating that the thermal degradation of the GDY/NC films is superior to that of pure NC.

The thermolysis process of NC was regarded to start from the breaking of the $-O-NO_2$ chemical bonds; the released NO_2 products remain in the polymer framework, then react with the free radicals or small molecule fragments (Benhammada et al. 2020; Katoh et al. 2010). In order to detect the functional groups and gaseous species of the GDY/NC

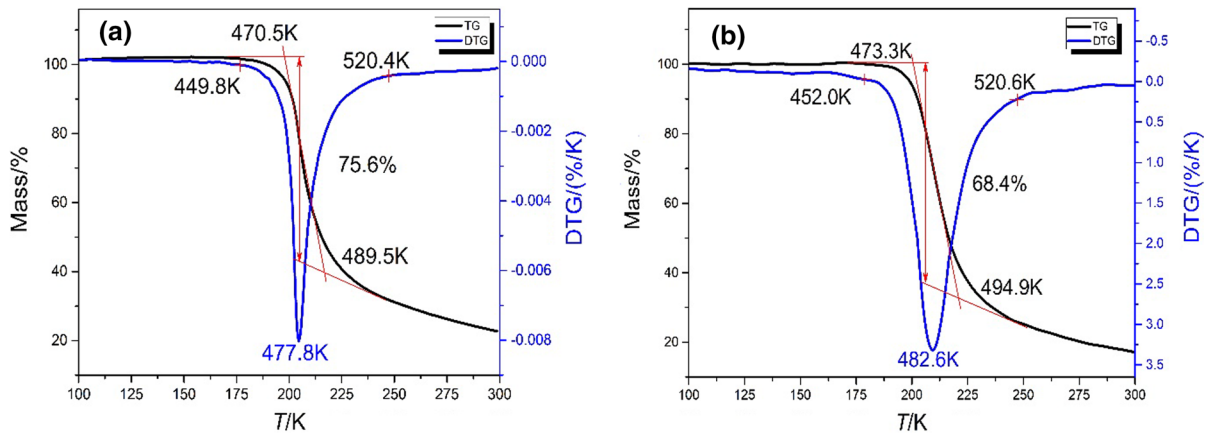


Fig. 8 TG/DTG curves of GDY/NC (a) and NC (b)

composites, the TG-IR-MS technique was adopted, and the corresponding results are shown in Fig. 9 and Fig. S2.

Figure 9a displays the IR spectra of the evolved gases at six typical temperatures points, namely T_i , T_o , T_p , T_e , T_f , and a specific temperature (T_x) below

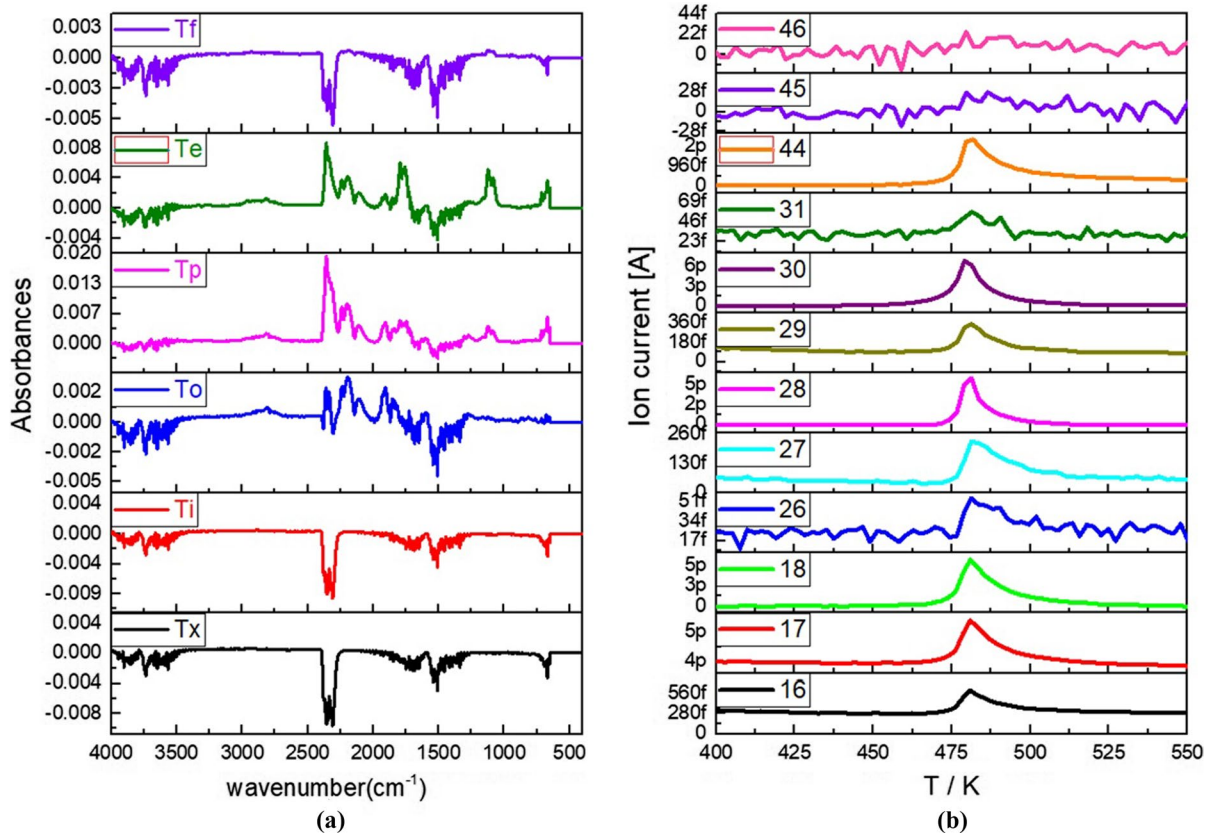


Fig. 9 IR (a) and MS (b) spectra of the gases evolved from the degradation of GDY/NC

the starting degradation temperature. When the GDY/NC composites were heated to 438.6 K (T_x), the IR absorption peaks of H₂O and CO₂ were detected at 3556–3732 cm⁻¹, and 2311–2356 cm⁻¹ respectively. Combining with the MS spectra shown in Fig. 9b, the signals corresponding to $m/z=18$ and $m/z=44$ are not observed, indicating that both H₂O and CO₂ originate from the environment and are not gaseous products resulting from the GDY/NC pyrolysis. The signals at 3564–3732 cm⁻¹ in the IR spectrum at 449.8 K (T_i) are attributed to the O–H stretching vibration frequencies of free water. The peaks at 2312–2360 cm⁻¹ and 666 cm⁻¹ correspond to the stretching vibration and bending vibration modes of CO₂, respectively. Based on the MS analysis presented in Fig. 9b, it can also be confirmed that free water and carbon dioxide are not the decomposition products of GDY/NC at the initial stage. It must be pointed out that the IR characteristic absorption peak of NO₂ (1582–1637 cm⁻¹) is very weak and can thus be neglected. The GDY/NC composites exhibit a slight ionic current variation for the $m/z=46$ (NO₂) fragment at 449.8 K. This phenomenon may be caused by the three-dimensional porous carbon networks composed of high π -conjugated acetylenic linkages, which may exhibit strong adsorption to NO₂.

Being a strong oxidizing agent, the NO₂ gas could further react with the free radicals to generate other products. Distinct spectral changes can be demonstrated at 470.5 K (T_o), the major gaseous products of GDY/NC include H₂O (3565–3730 cm⁻¹; $m/z=18$), CO₂ (2311–2380, 673 cm⁻¹; $m/z=44$), NO₂ (1570–1637 cm⁻¹; $m/z=46$) (Li et al. 2012; Wang et al. 2016), N₂O (2247 cm⁻¹; $m/z=44$), NO (1854–1910 cm⁻¹; $m/z=30$), CO (2191 cm⁻¹; $m/z=28$), HCN (2247 cm⁻¹; $m/z=27$), and HCHO (2695–2962 cm⁻¹; $m/z=30$) (Gratien et al. 2007). As shown in Fig. 9a, the peak intensities of all detected gases are very weak in the IR spectrum heated to this temperature. For the IR spectrum of GDY/NC at the peak temperature (477.8 K, T_p), the main released gas products during the GDY/NC pyrolysis are H₂O, CO₂, NO₂, NO, N₂O, CO, HCHO, HCOOH (1109 cm⁻¹) and HCN. The bands at 2695–2962 cm⁻¹ are attributed to the stretching vibration modes of the C–H bonds and C=O bonds of the HCHO molecules, respectively, due to the rupture of the –CH₂ONO₂ groups (Zhao et al. 2021). The HCOOH molecules originate from the

secondary autocatalytic reactions of NC (Shehata et al. 2003). The HCN (2247 cm⁻¹) molecules may be produced by the reaction between the ·CHO fragment with NO. At 489.5 K (T_e), the characteristic bands located at 1110 cm⁻¹, 1562–1635 cm⁻¹, 1772–1935 cm⁻¹, 2143–2198 cm⁻¹, 2241–2265 cm⁻¹, 2243 cm⁻¹, 2295–2385 cm⁻¹, 2726–2921 cm⁻¹, and 3509–3735 cm⁻¹ are attributed to HCOOH, NO₂, NO, CO, HCN, N₂O, CO₂, HCHO and H₂O, respectively. In particular, Fig. 9(a, T_p) shows that the intensities of the NO and HCOOH signals increase trend with the pyrolysis temperature, which indicates that the reaction between NO₂ and HCHO can be accelerated through the addition of GDY. When the GDY/NC thermolysis proceeded to the ending stage (Fig. 9(a, T_i)), NO₂, CO₂, HCOOH, H₂O, and HCN are still detected. These IR spectroscopy results are in good agreement with the MS data presented in Fig. 9b.

According to the TG-IR-MS analysis reported above, the possible thermolysis process of GDY/NC is briefly presented in Fig. 10. With the temperature increasing, GDY is effective in promoting the cleavages of the –O–NO₂ bonds and the glucopyranosyl rings to produce NO₂, H₂O, and CO₂ gases. These components especially NO₂ could further react with the condensed phase, free radicals or other fragments generated during NC degradation. The gases detected during the entire pyrolysis process of GDY/NC mainly contain H₂O, CO₂, HCN, N₂O, CO, NO₂, NO, HCHO, and HCOOH.

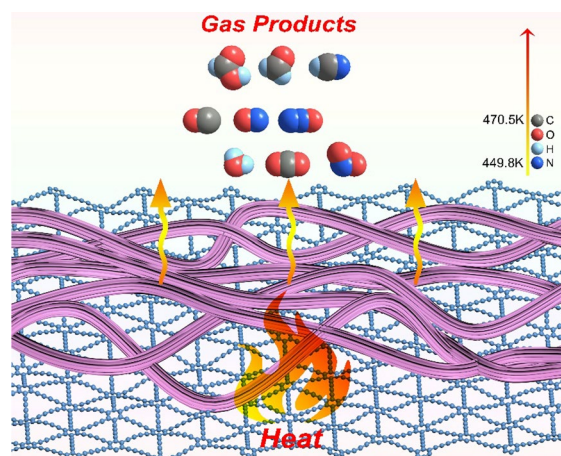


Fig. 10 Schematic illustration for the proposed thermal decomposition process of GDY/NC

Conclusion

In this work, the possibility of using a new type of intrinsic semiconducting carbon material with a bandgap (namely GDY) in the field of cellulose-derived energetic polymers is investigated for the first time. GDY was confirmed to possess an effective thermal catalytic activity and present the good compatibility with NC. Based on the DSC data obtained at six different heating rates, three general isoconversional approaches including FWO, KAS, and Friedman equations were employed to obtain the kinetic triplets. However, the poor linearity of the KCE revealed that the L2 and D3 models are not suitable to accurately describe the pyrolysis reactions of GDY/NC and NC. Furthermore, the n -th order modified models were adopted to describe the multistep pyrolysis reactions of GDY/NC and NC in order to obtain a good fit of the experimental data. It was demonstrated that, as a promising all-carbon catalyst, GDY can help NC to overcome the energy barrier, drive both the $-O-NO_2$ bond breaking during the initial process of the NC thermolysis and the condensed-phase decomposition, and increase the heat release. The TG-IR-MS analysis confirmed that the pyrolysis process of the GDY/NC complexes is different from that of pristine NC, which may be attributed to the microstructure and chemical bonds of GDY. In summary, this work reports the catalytic effect of GDY on the NC thermolysis, and provides insights into a potential GDY-based catalyst for use in the field of energetic materials.

Acknowledgments This work was supported by National Natural Science Foundation of China (Nos. 21673179 and 21978232), Program for the Doctoral Scientific Research Foundation of Xi'an University of Technology (No. 109-451117004), Natural Science Basic Research Program of Shaanxi (Nos. 2018JQ2077, 2018GY-125, 2019NY-201 and 2021JM-322), and Scientific Research Project of Shaanxi Provincial Department of Education (No. 19JK0595).

Funding The authors have not disclosed any funding.

Declarations

Conflict of interest The authors declare that they have no known competing financial interests or personal relationships that could have appeared to influence the work reported in this paper.

References

- Akahira T, Sunose T (1971) Method of determining activation deterioration constant of electrical insulating materials. *Res Rep Chiba Inst Technol (sci Technol)* 16:22–31
- Ahlawat J, Asil SM, Barroso GG, Nurunnabi M, Narayan M (2020) Application of carbon nano onions in the biomedical field: recent advances and challenges. *Biomater Sci-UK* 9(3):626–644. <https://doi.org/10.1039/d0bm01476a>
- Ashery A, Farag AAM, Moussa MA, Turky GM (2020) Enhancement of electrical and dielectrically performance of graphene-based promise electronic devices. *Synthetic Met* 261:116303. <https://doi.org/10.1016/j.synthmet.2020.116303>
- Beach NE, Canfield VK (1971) Compatibility of explosive with polymers (III). *Plastic Rep* 40:73–76
- Benhammada A, Trache D, Kesraoui M, Tarchoun AF, Chelouche S, Mezroua A (2020) Synthesis and characterization of α -Fe₂O₃ nanoparticles from different precursors and their catalytic effect on the thermal decomposition of nitrocellulose. *Thermochim Acta* 686:178570. <https://doi.org/10.1016/j.tca.2020.178570>
- Benhammada A, Trache D (2020) Thermal decomposition of energetic materials using TG-FTIR and TG-MS: a state-of-the-art review. *Appl Spectrosc Rev* 55(8):724–777. <https://doi.org/10.1080/05704928.2019.1679825>
- Benhammada A, Trache D (2022) Green synthesis of CuO nanoparticles using Malva sylvestris leaf extract with different copper precursors and their effect on nitrocellulose thermal behavior. *J Therm Anal Calorim* 147:1–16. <https://doi.org/10.1007/s10973-020-10469-5>
- Cai J, Xu D, Dong Z, Yu X, Yang Y, Banks SW, Bridgwater AV (2018) Processing thermogravimetric analysis data for isoconversional kinetic analysis of lignocellulosic biomass pyrolysis: Case study of corn stalk. *Renew Sust Energ Rev* 82:2705–2715. <https://doi.org/10.1016/j.rser.2017.09.113>
- Chai H, Duan Q, Jiang L, Gong L, Chen H, Sun J (2019) Theoretical and experimental study on the effect of nitrogen content on the thermal characteristics of nitrocellulose under low heating rates. *Cellulose* 26(2):763–776. <https://doi.org/10.1007/s10570-018-2100-0>
- Chelouche S, Trache D, Tarchoun AF, Abdelaziz A, Khimeche K (2019a) Compatibility assessment and decomposition kinetics of nitrocellulose with eutectic mixture of organic stabilizers. *J Energ Mater* 38(1):48–67. <https://doi.org/10.1080/07370652.2019.1661543>
- Chelouche S, Trache D, Tarchoun AF, Khimeche K, Mezroua A (2019b) Compatibility of nitrocellulose with aniline-based compounds and their eutectic mixtures. *J Therm Anal Calorim* 141(2):941–955. <https://doi.org/10.1007/s10973-019-09048-0>
- Chen HH, Ma WL, Huang ZY, Zhang Y, Huang Y, Chen YS (2019a) Graphene-based materials toward microwave and terahertz absorbing stealth technologies. *Adv Opt Mater* 7(8):1801318. <https://doi.org/10.1002/adom.201801318>
- Chen T, Du P, Jiang W, Liu J, Hao GZ, Gao H, Xiao L, Ke X, Zhao FQ, Xuan CL (2016) A facile one-pot

- solvothermal synthesis of $\text{CoFe}_2\text{O}_4/\text{RGO}$ and its excellent catalytic activity on thermal decomposition of ammonium perchlorate. *RSC Adv* 6(87):83838–83847. <https://doi.org/10.1039/c6ra16448j>
- Chen Y, Li J, Wang F, Guo J, Jiu T, Liu H (2019b) Chemical modification: toward solubility and processability of graphdiyne. *Nano Energy* 64:103932. <https://doi.org/10.1016/j.nanoen.2019.103932>
- Chen YW, Zhang HY, Zeng GX (2018) Tunable and high performance electromagnetic absorber based on ultralight 3D graphene foams with aligned structure. *Carbon* 140:494–503. <https://doi.org/10.1016/j.carbon.2018.09.014>
- Cui M, Hu TT, Chen LL, Li P, Gong YH, Wu ZX, Wang S (2020) Recent progress in graphdiyne for electrocatalytic reactions. *ChemElectroChem* 7(24):4843–4852. <https://doi.org/10.1002/celec.202001313>
- Flynn JH, Wall LA (1966) A quick, direct method for the determination of activation energy from thermogravimetric data. *J Polym Sci Part C: Polym Lett* 4(5):323–328. <https://doi.org/10.1002/pol.1966.110040504>
- Friedman HL (1964) Kinetics of thermal degradation of char-forming plastics from thermogravimetry. Application to a phenolic plastic. *J Polym Sci Part C Polym Symp* 6(1):183–195. <https://doi.org/10.1002/polc.5070060121>
- Gao L, Ge X, Zuo Z, Wang F, Liu X, Lv M, Shi S, Xu L, Liu T, Zhou Q, Ye X, Xiao S (2020a) High quality pyrazinoquinoxaline-based graphdiyne for efficient gradient storage of lithium ions. *Nano Lett* 20(10):7333–7341. <https://doi.org/10.1021/acs.nanolett.0c02728>
- Gao X, Jiang L, Xu Q (2020b) Experimental and theoretical study on thermal kinetics and reactive mechanism of nitrocellulose pyrolysis by traditional multi kinetics and modeling reconstruction. *J Hazard Mater* 386:121645. <https://doi.org/10.1016/j.jhazmat.2019.121645>
- Gratien A, Nilsson E, Doussin JF, Johnson MS, Nielsen CJ, Stenström Y, Picquet-Varrault B (2007) UV and IR absorption cross-sections of HCHO, HCDO, and DCDO. *J Phys Chem A* 111(45):11506–11513. <https://doi.org/10.1021/jp074288r>
- Guo Y, Zhao N, Zhang T, Gong H, Ma H, An T, Zhao F, Hu R (2019) Compatibility and thermal decomposition mechanism of nitrocellulose/ Cr_2O_3 nanoparticles studied using DSC and TG-FTIR. *RSC Adv* 9:3927–3937. <https://doi.org/10.1039/c8ra09632e>
- Hao BW, Deng ZM, Bi SG, Ran JH, Cheng DS, Luo L, Cai GM, Wang X, Tang XN (2021) In situ polymerization of pyrrole on CNT/cotton multifunctional composite yarn for supercapacitors. *Ionics* 27(1):279–288. <https://doi.org/10.1007/s11581-020-03784-2>
- He J, Wang N, Cui Z, Du H, Fu L, Huang C, Yang Z, Shen X, Yi Y, Tu Z, Li Y (2017) Hydrogen substituted graphdiyne as carbon-rich flexible electrode for lithium and sodium ion batteries. *Nat Commun* 8(1):1172. <https://doi.org/10.1038/s41467-017-01202-2>
- Katoh K, Higashi E, Nakano K, Ito S, Wada Y, Kasamatsu J, Miya H, Yamamoto M, Wada Y (2010) Thermal behavior of nitrocellulose with inorganic salts and their mechanistic action. *Propell Explos Pyrotech* 35(5):461–467. <https://doi.org/10.1002/prop.200900074>
- Khawam A, Flanagan DR (2006) Solid-state kinetic models: basics and mathematical fundamentals. *J Phys Chem B* 110(35):17315–17328. <https://doi.org/10.1021/jp062746a>
- Kim KJ, Jung H, Kim JH, Jang NS, Kim JM, Kim SH (2017) Nanoenergetic material-on-multiwalled carbon nanotubes paper chip as compact and flexible igniter. *Carbon* 114:217–223. <https://doi.org/10.1016/j.carbon.2016.12.021>
- Kissinger HE (1957) Reaction kinetics in differential thermal analysis. *Anal Chem* 29(11):1702–1706. <https://doi.org/10.1021/ac60131a045>
- Koo B, Byun S, Nam SW, Moon SY, Kim S, Park JY, Ahn BT, Shin B (2018) Reduced graphene oxide as a catalyst binder: greatly enhanced photoelectrochemical stability of Cu(In, Ga) S_2 photocathode for solar water splitting. *Adv Funct Mater* 28(16):1705136. <https://doi.org/10.1002/adfm.201705136>
- Li G, Li Y, Liu H, Guo Y, Li Y, Zhu D (2010) Architecture of graphdiyne nanoscale films. *Chem Commun* 46:3256–3258. <https://doi.org/10.1039/b922733d>
- Li X, Lin Q, Zhao XY, Han ZW, Wang B (2016) Compatibility of 2, 4, 6, 8, 10,12-Hexanitrohexaazaisowurtzitane with a selection of insensitive explosives. *J Energ Mater* 35(2):188–196. <https://doi.org/10.1080/07370652.2016.1245372>
- Li Y, Chenxia K, Huang C, Cheng Y (2012) Effect of MnC_2O_4 nanoparticles on the thermal decomposition of TEGDN/NC propellant. *J Therm Anal Calorim* 109:171–176. <https://doi.org/10.1007/s10973-011-1694-3>
- Lin Y, Kang H, Liang M, Ye X, Li J, Feng Q, Zheng Y, Huang Z (2020) Hybrid nanostructured MnO_2 nanowire/graphdiyne with enhanced lithium-ion performance promoting by interfacial storage. *Appl Surf Sci* 526:146457. <https://doi.org/10.1016/j.apsusc.2020.146457>
- Liu J, Wang L, Shen X, Gao X, Chen Y, Liu H, Liu Y, Yin D, Liu Y, Xu W, Cai R, You M, Guo M, Wang Y, Li J, Li Y, Chen C (2020) Graphdiyne-templated palladium-nanoparticle assembly as a robust oxygen generator to attenuate tumor hypoxia. *Nano Today* 34:100907. <https://doi.org/10.1016/j.nantod.2020.100907>
- Liu XY, Lu J, Jiang JL, Jiang Y, Gao Y, Li WR, Zhao B, Zhang JJ (2021a) Enhancing lithium storage performance by strongly binding silicon nanoparticles sandwiching between spherical graphene. *Appl Surf Sci* 539:148191. <https://doi.org/10.1016/j.apsusc.2020.148191>
- Liu Y, Xue Y, Yu H, Hui L, Huang B, Li Y (2021b) Graphdiyne ultrathin nanosheets for efficient water splitting. *Adv Funct Mater* 31(16):2010112. <https://doi.org/10.1002/adfm.202010112>
- Lv Y, Wu XY, Jia W, Guo JX, Zhang HB, Liu HB, Jia DZ, Tong FL (2020) Graphdiyne-anchored ultrafine NiFe hydroxide nanodots electrocatalyst for water oxidation with high mass activity and superior durability. *Carbon* 169:45–54. <https://doi.org/10.1016/j.carbon.2020.07.048>
- Ma JP, Yuan Y, Wu S, Lee JY, Kang BT (2020) γ -Graphyne nanotubes as promising lithium-ion battery anodes. *Appl Surf Sci* 531:147343. <https://doi.org/10.1016/j.apsusc.2020.147343>
- Ma JY, Xing MD, Yin LW, Hui KS, Hui KN (2021) Porous hierarchical $\text{TiO}_2/\text{MoS}_2/\text{RGO}$ nanoflowers as anode material for sodium ion batteries with high capacity and

- stability. *Appl Surf Sci* 536:147735. <https://doi.org/10.1016/j.apsusc.2020.147735>
- Ma ZL, Qi L, He W, He LM (2019) A novel approach on the study of cure kinetics for rheological isothermal and non-isothermal methods. *Compos Part B-Eng* 162:242–249. <https://doi.org/10.1016/j.compositesb.2018.10.066>
- Mahdizadeh SJ, Goharshadi EK (2020) Multicomponent gas separation and purification using advanced 2D carbonaceous nanomaterials. *RSC Adv* 10(41):24255–24264. <https://doi.org/10.1039/d0ra04286b>
- Ozawa T (1965) A new method of analyzing thermogravimetric data. *Bull Chem Soc Jpn* 38(11):1881–1886. <https://doi.org/10.1246/bcsj.38.1881>
- Samantaray SS, Sangeetha V, Abinaya S, Ramaprabhu S (2020) Diatom frustule-graphene based nanomaterial for room temperature hydrogen storage. *Int J Hydrogen Energy* 45(1):764–773. <https://doi.org/10.1016/j.ijhydene.2019.10.155>
- Sánchez-Jiménez PE, Pérez-Maqueda LA, Perejón A, Criado JM (2010a) Generalized kinetic master plots for the thermal degradation of polymers following a random scission mechanism. *J Phys Chem A* 114:7868–7876. <https://doi.org/10.1021/jp103171h>
- Sánchez-Jiménez PE, Pérez-Maqueda LA, Perejón A, Criado JM (2010b) A new model for the kinetic analysis of thermal degradation of polymers driven by random scission. *Polym Degrad Stab* 95(5):733–739. <https://doi.org/10.1016/j.polymdegradstab.2010.02.017>
- Sánchez-Jiménez PE, Pérez-Maqueda LA, Perejón A, Criado JM (2011) Constant rate thermal analysis for thermal stability studies of polymers. *Polym Degrad Stab* 96(5):974–981. <https://doi.org/10.1016/j.polymdegradstab.2011.01.027>
- Sánchez-Jiménez PE, Pérez-Maqueda LA, Perejón A, Criado JM (2013) Generalized master plots as a straightforward approach for determining the kinetic model: the case of cellulose pyrolysis. *Thermochim Acta* 552:54–59. <https://doi.org/10.1016/j.tca.2012.11.003>
- Shehata AB, Hassan MA, Nour MA (2003) Effect of new poly 2-acryloyl-n, n'-bis (4-nitrophenyl) propan diamide and poly 2-acryloyl-n, n'-bis (4-methylphenyl) propan diamide and their synergistic action on the stability of nitrocellulose. *J Hazard Mater* 102(2–3):121–136. [https://doi.org/10.1016/S0304-3894\(03\)00138-9](https://doi.org/10.1016/S0304-3894(03)00138-9)
- Shi MM, Bi L, Huang X, Meng ZS, Wang YH, Yang ZH (2020a) Design of three-dimensional nanotube-fullerene-interconnected framework for hydrogen storage. *Appl Surf Sci* 534:147606. <https://doi.org/10.1016/j.apsusc.2020.147606>
- Shi G, Xie Y, Du L, Fan Z, Chen X, Fu X, Xie W, Wang M, Yuan M (2020b) Stabilization of cobalt clusters with graphdiyne enabling efficient overall water splitting. *Nano Energy* 74:104852. <https://doi.org/10.1016/j.nanoen.2020.104852>
- Smeu M, Zahid F, Ji W, Guo H, Jaidann M, Abou-Rachid H (2011) Energetic molecules encapsulated inside carbon nanotubes and between graphene layers: DFT calculations. *J Phys Chem C* 115(22):10985–10989. <https://doi.org/10.1021/jp201756p>
- Song B, Chen M, Zeng GM, Gong JL, Shen MC, Xiong WP, Zhou CY, Tang X, Yang Y, Wang WJ (2020) Using graphdiyne (GDY) as a catalyst support for enhanced performance in organic pollutant degradation and hydrogen production: a review. *J Hazard Mater* 398:122957. <https://doi.org/10.1016/j.jhazmat.2020.122957>
- Sun MZ, Wu T, Dougherty AW, Lam MG, Huang BL, Li YL, Yan CH (2021) Self-validated machine learning study of graphdiyne-based dual atomic catalyst. *Adv Energy Mater* 11(13):2003796. <https://doi.org/10.1002/aenm.202003796>
- Tarchoun AF, Trache D, Klapötke TM, Chelouche S, Derradji M, Bessa W, Mezroua A (2019) A promising energetic polymer from *Posidonia oceanica* brown algae: synthesis, characterization, and kinetic modeling. *Macromol Chem Phys* 220(22):1900358. <https://doi.org/10.1002/macp.201900358>
- Tarchoun AF, Trache D, Klapötke TM, Belmerabet M, Abdelaziz A, Derradji M, Belgacemi R (2020a) Synthesis, characterization, and thermal decomposition kinetics of nitrogen-rich energetic biopolymers from aminated giant reed cellulosic fibers. *Ind Eng Chem Res* 59(52):22677–22689. <https://doi.org/10.1021/acs.iecr.0c05448>
- Tarchoun AF, Trache D, Klapötke TM, Khimeche K (2020b) Tetrazole-functionalized microcrystalline cellulose: a promising biopolymer for advanced energetic materials. *Chem Eng J* 400:125960. <https://doi.org/10.1016/j.cej.2020.125960>
- Tarchoun AF, Trache D, Klapötke TM, Krumm B, Khimeche K, Mezroua A (2020c) A promising energetic biopolymer based on azide-functionalized microcrystalline cellulose: synthesis and characterization. *Carbohydr Polym* 249:116820. <https://doi.org/10.1016/j.carbpol.2020.116820>
- Tarchoun AF, Trache D, Klapötke TM, Krumm B, Kofen M (2021a) Synthesis and characterization of new insensitive and high-energy dense cellulosic biopolymers. *Fuel* 292:120347. <https://doi.org/10.1016/j.fuel.2021.120347>
- Tarchoun AF, Trache D, Klapötke TM, Selmani A, Saada M, Chelouche S, Mezroua A, Abdelaziz A (2021b) New insensitive high-energy dense biopolymers from giant reed cellulosic fibers: their synthesis, characterization, and non-isothermal decomposition kinetics. *New J Chem* 45:5099–5113. <https://doi.org/10.1039/D0NJ05484D>
- Tarchoun AF, Trache D, Klapötke TM, Abdelaziz A, Derradji M, Bekhouche S (2022) Chemical design and characterization of cellulosic derivatives containing high-nitrogen functional groups: Towards the next generation of energetic biopolymers. *Def Technol* 18:537–546. <https://doi.org/10.1016/j.dt.2021a.03.009>
- van der Heijden AEDM, Bouma RHB, van der Steen AC, Fischer HR (2003) Application and characterization of nanomaterials in energetic compositions. *MRS Online Proc Libr* 800:203–220. <https://doi.org/10.1557/PROC-800-AA5.6>
- Vyazovkin S (2018) Modern isoconversional kinetics: from misconceptions to advances - ScienceDirect. *Handbook Therm Anal Calorim* 6:131–172. <https://doi.org/10.1016/B978-0-444-64062-8.00008-5>
- Vyazovkin S, Burnham AK, Criado JM, Pérez-Maqueda LA, Popescu C, Sbirrazzuoli N (2011) ICTAC Kinetics Committee recommendations for performing kinetic computations on thermal analysis data. *Thermochim Acta* 520:1–19. <https://doi.org/10.1016/j.tca.2011.03.034>

- Wang R, Shi M, Xu F, Qiu Y, Zhang P, Shen K, Zhao Q, Yu J, Zhang Y (2020) Graphdiyne-modified TiO₂ nanofibers with osteoinductive and enhanced photocatalytic antibacterial activities to prevent implant infection. *Nat Commun* 11(1):4465. <https://doi.org/10.1038/s41467-020-18267-1>
- Wang YL, Zhao FQ, Yi JH (2012a) New progress of study combustion catalysts used for solid rocket propellants. *Chin J Explos Propellants* 35:1–8
- Wang S, Yi L, Halpert JE, Lai X, Liu Y, Cao H, Yu R, Wang D, Li Y (2012b) A novel and highly efficient photocatalyst based on P25-graphdiyne nanocomposite. *Small* 8:265–271. <https://doi.org/10.1002/sml.201101686>
- Wang Y, Song X, Song D, Liang L, An C, Wang J (2016) Synthesis, thermolysis, and sensitivities of HMX/NC energetic nanocomposites. *J Hazard Mater* 312:73–83. <https://doi.org/10.1016/j.jhazmat.2016.03.043>
- Wong SI, Lin H, Yang YY, Sunarso J, Wong BT, Jia BH (2020) Tailoring reduction extent of flash-reduced graphene oxides for high performance supercapacitors. *J Power Sources* 478:228732. <https://doi.org/10.1016/j.jpowsour.2020.228732>
- Xu JC, Bian YC, Liu Y, Zhai D (2017a) Reactive molecular dynamics study of thermal decomposition of nanocarbon energetic composite materials. *Comput Mater Sci* 131:126–131. <https://doi.org/10.1016/j.commatsci.2017.01.044>
- Xu L, Jiang Y, Wang L (2017b) Thermal decomposition of rape straw: pyrolysis modeling and kinetic study via particle swarm optimization. *Energ Convers Manage* 146:124–133. <https://doi.org/10.1016/j.enconman.2017.05.020>
- Xue YR, Guo Y, Yi YP, Li YJ, Liu HB, Li D, Yang WS, Li YL (2016) Self-catalyzed growth of Cu@graphdiyne core-shell nanowires array for high efficient hydrogen evolution cathode. *Nano Energy* 30:858–866. <https://doi.org/10.1016/j.nanoen.2016.09.005>
- Yan QL, Li XJ, Zhang LY, Li JZ, Li HL, Liu ZR (2008) Compatibility study of trans-1,4,5,8-tetranitro-1,4,5,8-tetraazadecalin (TNAD) with some energetic components and inert materials. *J Hazard Mater* 160(2–3):529–534. <https://doi.org/10.1016/j.jhazmat.2008.03.027>
- Yao E, Zhao N, Qin Z, Ma H, Li H, Xu S, An T, Yi J, Zhao F (2020) Thermal decomposition behavior and thermal safety of nitrocellulose with different shape CuO and Al/CuO nanothermites. *Nanomaterials* 10:725. <https://doi.org/10.3390/nano10040725>
- Yi H, Huang DL, Qin L, Zeng GM, Lai C, Cheng M, Ye SJ, Song B, Ren XY, Guo XY (2018) Selective prepared carbon nanomaterials for advanced photocatalytic application in environmental pollutant treatment and hydrogen production. *Appl Catal B-Environ* 239:408–424. <https://doi.org/10.1016/j.apcatb.2018.07.068>
- Yin X-P, Tang S-F, Zhang C, Wang H-J, Si R, Lu X-L, Lu T (2020) Graphdiyne-based Pd single-atom catalyst for semi-hydrogenation of alkynes to alkenes with high selectivity and conversion under mild conditions. *J Mater Chem A* 8(40):20925–20930. <https://doi.org/10.1039/d0ta07705d>
- Yuan Y, Jiang W, Wang YJ, Shen P, Li FS, Li PY, Zhao FQ, Gao HX (2014) Hydrothermal preparation of Fe₂O₃/graphene nanocomposite and its enhanced catalytic activity on the thermal decomposition of ammonium perchlorate. *Appl Surf Sci* 303:354–359. <https://doi.org/10.1016/j.apsusc.2014.03.005>
- Zeng J, Zhao N, Zhang T, Yao E, Zhao F, Ren Y, Ma H (2021) Thermal decomposition of graphdiyne/RDX composites. *Chinese J Explos Propell* 44(4):474–483
- Zhang SC, Kang LX, Wang X, Tong LM, Yang LW, Wang ZQ, Qi K, Deng SB, Li QW, Bai XD, Ding F, Zhang J (2017a) Arrays of horizontal carbon nanotubes of controlled chirality grown using designed catalysts. *Nature* 543:234–238. <https://doi.org/10.1038/nature21051>
- Zhang T, Zhao N, Li J, Gong H, An T, Zhao F, Ma H (2017b) Thermal behavior of nitrocellulose-based superthermites: effects of nano-Fe₂O₃ with three morphologies. *RSC Adv* 7:23583–23590. <https://doi.org/10.1039/c6ra28502c>
- Zhang X, Hikal WM, Zhang Y, Bhattacharia SK, Li L, Panditrao S, Wang SR, Weeks BL (2013) Direct laser initiation and improved thermal stability of nitrocellulose/graphene oxide nanocomposites. *Appl Phys Lett* 102(14):141905. <https://doi.org/10.1063/1.4801846>
- Zhang YH, Shao ZQ, Gao KZ, Wu X, Liu YH (2014) Tensile properties of nitrate glycerol ethercellulose/graphene oxide nanocomposites. *Integr Ferroelectr* 154(1):147–153. <https://doi.org/10.1080/10584587.2014.904717>
- Zhao FQ, Yi JH, Hong WL, An T, Yang YJ (2016a) Preparation, characterization, and catalytic activity of carbon nanotubes-supported metal or metal oxide. *Energ Nanomaterials*. <https://doi.org/10.1016/B978-0-12-802710-3.00010-6>
- Zhao N, Li J, Gong H, An T, Zhao F, Yang A, Hu R, Ma H (2016b) Effects of α -Fe₂O₃ nanoparticles on the thermal behavior and non-isothermal decomposition kinetics of nitrocellulose. *J Anal Appl Pyrol* 120:165–173. <https://doi.org/10.1016/j.jaap.2016b.05.002>
- Zhao N, Li J, Zhao F, An T, Hu R, Ma H (2016c) Combustion catalyst: nano-Fe₂O₃ and nano-thermite Al/Fe₂O₃ with different shapes. *Dev Combustion Technol*. <https://doi.org/10.5772/64748>
- Zhao N, Ma H, Yao E, Yu Z, An T, Zhao F, Yu X (2021) Influence of tailored CuO and Al/CuO nanothermites on the thermocatalytic degradation of nitrocellulose and combustion performance of AP/HTPB composite propellant. *Cellulose* 28:8671–8691. <https://doi.org/10.1007/s10570-021-04060-w>
- Zhou XP, Meng T, Yi FY, Shu D, Han DM, Zhu ZH, Gao AM, Liu C, Li X, Yang KM, Yi H (2020) Supramolecular-induced confining methylene blue in three-dimensional reduced graphene oxide for high-performance supercapacitors. *J Power Sources* 475:228554. <https://doi.org/10.1016/j.jpowsour.2020.228554>
- Zu YQ, Zhang Y, Xu KZ, Zhao FQ (2016) Graphene oxide-MgWO₄ nanocomposite as an efficient catalyst for the thermal decomposition of RDX, HMX. *RSC Adv* 37(6):31046–31052. <https://doi.org/10.1039/c6ra05101d>
- Zuo Z, Shang H, Chen Y, Li J, Liu H, Li Y, Li Y (2017) A facile approach for graphdiyne preparation under atmosphere for an advanced battery anode. *Chem Commun* 53(57):8074–8077. <https://doi.org/10.1039/c7cc03200e>

Publisher's Note Springer Nature remains neutral with regard to jurisdictional claims in published maps and institutional affiliations.